Antihypertensive Drug Valsartan in Solution and at the AT_1 Receptor: Conformational Analysis, Dynamic NMR Spectroscopy, *in Silico* Docking, and Molecular Dynamics Simulations

Constantinos Potamitis,[†,⊥] Maria Zervou,[†] Vassilis Katsiaras,[†] Panagiotis Zoumpoulakis,[†] Serdar Durdagi,[†,‡] Manthos G. Papadopoulos,[†] Joseph M. Hayes,[†] Simona Golic Grdadolnik,[§] Ioanna Kyrikou,[†] Dimitris Argyropoulos,[||] Georgia Vatougia,[†] and Thomas Mavromoustakos*[,†,⊥,#]

National Hellenic Research Foundation, Institute of Organic and Pharmaceutical Chemistry, Vas, Constantinou 48, 11635, Athens, Greece, Department of Biology Chemistry and Pharmacy, Free University of Berlin, Takustrasse, 3, 14195 Berlin, Germany, Laboratory of Biomolecular Structure, National Institute of Chemistry, Hajdrihova 19, POB 30 SI-1115 Ljubljana, Slovenia, Varian Ltd., 10 Mead Road, Oxford Industrial Park, Yarnton, Oxford OX5 1QU, United Kingdom, Chemistry Department, National & Kapodistrian University of Athens, Zographou 15784, Athens, Greece, and Center of Applied Research and Technology, Nicosia, Cyprus, 46 Makedonitissas Avenue, 1700 Nicosia, Cyprus

Received November 21, 2008

The conformational properties of AT_1 antagonist valsartan have been analyzed both *in solution* and at the binding site of the receptor. Low energy conformations of valsartan *in solution* were explored by NMR spectroscopy and molecular modeling studies. The NMR results showed the existence of two distinct and almost isoenergetic conformations for valsartan (*cis:trans* ratio around the amide bond ~40:60) that coalesce at the temperature range of 55−60 °C in agreement with previous *in solution* conformational analysis study (Fang et al. *Magn. Reson. Chem.* **2007**, *45*, 929−936). Quantum mechanics and ONIOM calculations revealed that the bulky valsartan substituents actually contribute to stabilization of the transition state for interconversion. *In silico* docking and Molecular Dynamic studies were applied to study binding of valsartan at the AT_1 receptor site models, explicitly solvated and embedded in lipid bilayers and solvent molecules. These studies revealed that the majority of docked poses adopted a *trans* (major) conformation. Of paramount and maybe biological importance are the MD simulations results which showed that the two acidic groups of valsartan are bridged through LYS199 enabling it for multiple hydrogen bond interactions. In a lipid bilayer environment these interactions are enhanced, designating the important role of lipid bilayers for the better binding of valsartan and its stabilization at the active site.

INTRODUCTION

Angiotensin II (AII), a potent vasoconstrictive hormone formed within the RAS cascade, is implicated in the increase of the arterial blood pressure. Drug design for developing novel synthetic antihypertensive drugs were targeted either to the inhibition of AII biosynthesis (renin or angiotensin converting enzyme (ACE) inhibitors) or to the antagonism of AII binding to Angiotensin II (AT_1) receptors.[1] Angiotensin II receptor blockers (ARBs) have been developed to produce a more complete blockade of the action of AII compared to other drug classes as well as an improved side effect profile.[2]

The first AT_1 antagonists were peptide analogs which despite their poor bioavailability aided in the extraction of valuable SAR results. Losartan (Cozaar) was the first successful peptidomimetic analog to be marketed against hypertension. Valsartan (Diovan) whose structure is shown in Figure 1 is the second orally active nonpeptide AII antagonist administered for the regulation of high blood pressure.[3−9] Recent studies have shown the benefits of valsartan in other diseases such as heart failure, postmyocardial infarction, and hypertensive diabetic nephropathy with proteinuria and left ventricular hypertrophy, anti-inflamma-

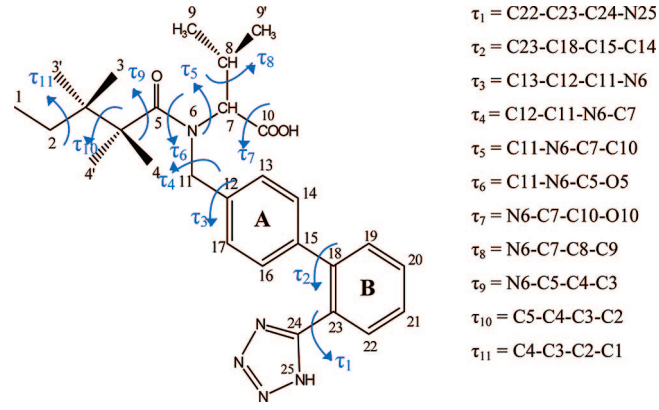

Figure 1. Valsartan and its critical dihedral angles that determine its conformational properties. Major and minor conformations are defined by (τ_6) with corresponding *trans* and *cis* dihedral angles.

* Corresponding author phone: +30 2107273869 or 2107274293; fax: +30 2107273831 or 2107274261; e-mail: tmavro@eie.gr and tmavrom@chem.uoa.gr.
† National Hellenic Research Foundation.
⊥ Kapodistrian University of Athens.
‡ Free University of Berlin.
§ National Institute of Chemistry.
|| Varian Ltd.
Center of Applied Research and Technology.

10.1021/ci800427s CCC: $40.75
Published on Web 03/03/2009

tory and antioxidative properties which may inhibit the development of atherosclerosis by lowering serum pro-inflammatory cytokines.[10−12]

The design of losartan was based on the C-terminal segment mimicry of the AII conformational model proposed by Fermadjian et al.[13] Superimposition revealed equivalent pharmocophoric segments between the C-terminal group of AII and losartan.[14] Valsartan's rational design was based on previous superimposition studies of losartan with the C-terminal segment of [Sar(1), Ile(8)]AII and the hypothesis that the imidazole ring of losartan mimics the amide bond between Ile(5) and His(6). This finding led to the replacement of the heterocycle group with an alkylated amino acid. Superimposition studies of valsartan with [Sar(1), Ile(8)]AII have shown that the butyl chain and the phenyl-tetrazole moieties correspond to the side chains of Pro(7) and Tyr(4), respectively.[14]

The following electrostatic potential inhibitor characteristics appear to be critical for AT_1 receptor recognition: (a) a positive long-range molecular electric potential (MEP) in the region of space surrounding the lipophilic side chain and (b) a strongly electrophile attracting region bulging out of the amide carbonyl moiety and the carboxylic group. The possibility of electrostatic discrimination among antagonists is related more to the overall topology of the electrostatic potential distribution.[15]

Our laboratory has been engaged in the study of the conformational properties of AT_1 antagonists already marketed as well as novel synthetic molecules. The aim of these studies is to understand the stereoelectronic properties responsible for drug activity and design new molecules with better biological profile.[16−33]

In a previous study theoretical calculations on the conformational exchange of valsartan and related compounds have been performed.[34] ^{1}H and ^{13}C NMR spectroscopy revealed the presence of two distinct conformations of valsartan (major symbolized with 'M' (trans) and minor symbolized with 'm' (cis)) (Figure 1) due to the hindered rotation of its amide bond, and the kinetic and thermodynamic parameters of the equilibrium between the two conformations are investigated using dynamic NMR spectroscopy. This finding is in accordance with other reported data in the literature, since the amide bond due to its resonance forms can hinder the bond rotation and thus generate conformers that can be observed in NMR time scale.[35,36]

In this study, dynamic NMR spectroscopy was applied in DMSO-d_6 solvent, and the results were compared with those published by Fang et al.,[34] performed in methanol solvent. In addition, the conformational analysis of valsartan at the binding site of the receptor and the role of membrane bilayer on conformations using *in silico* docking and MD simulations were investigated of both membrane associated and membrane free systems. Although the studies are performed in "artificial" biological conditions and may not reflect the true biological processes, they provide valuable data for the molecular basis of hypertension and can contribute to the rational design of novel analogues.

EXPERIMENTAL SECTION

1. NMR Spectroscopy. NMR spectra were recorded on a Varian INOVA 600 MHz spectrometer. The sample concentration used in NMR studies was *ca.* 10 mM dissolved in a mixture of DMSO-d_6/D_2O (1:1), the gradient selected version of the DQF-COSY. ^{1}H−^{13}C HSQC and ^{1}H−^{13}C HMBC experiments were used. The offset compensated 2D ROESY experiments were performed using a mixing time of 150 ms in the phase-sensitive mode along with 4 KHz spin-locking field strength and the WET sequence in order to suppress the water signal. The performance of a series of NOESY experiments using mixing times of 75 ms, 150 ms, 300 ms, and 1 s revealed a suitable mixing time of 150 ms that ensures the operation at the initial linear part of the NOE buildup curve. The ^{1}H spectral window used was 6000 Hz. The homonuclear 2D proton spectra were acquired with 4096 data points in t2 dimension, 32 scans, 256−512 points in t1 dimension, and a relaxation delay of 1−1.5 s. The ^{13}C spectral width was 30000 Hz. The ^{1}H−^{13}C heteronuclear experiments were acquired with 1024−4096 data points in t2 dimension and 32−64 scans and 256−512 points in t1 dimension. Experimental data were processed using VNMR routines. Spectra were zero-filled two times and were apodized using a squared cosine bell function in both dimensions. Interatomic proton−proton distances were calculated using the two-spin approximation, and the integrated cross peaks intensity of a pair of adjacent aromatic protons were assumed to have a distance of 2.46 Å. The resulting distances were corrected for the frequency offset effects to be eliminated.[37] Upper and lower limit values of constraints were allowed ±10% of toleration.

2D-EXSY experiments were performed on a Varian 600 MHz spectrometer. Spectra were acquired at three temperatures (20, 25, and 30 °C) using three mixing times (100, 150, and 200 ms) for each temperature. For each EXSY experiment acquired at a certain mixing time (t_m), the diagonal and the off diagonal traces corresponding to the signals in exchange are quantified. The selected mixing times lay in the linear part of the build-up curve assuring the accurate quantification of the diagonal and off diagonal traces corresponding to the signals in exchange. An EXSY experiment acquired with $t_m = 0$ ms, where no magnetization exchange occurs, was used as a reference experiment. The calculations of the rate constants were done importing the quantified EXSY data into EXSY CALC software of Mestrelab Research.[38]

^{13}C quantitative NMR experiments were run at the temperature range 20−70 °C on a BRUKER AC 300 MHz spectrometer using the Inverse Gate pulse sequence. A 90° pulse was applied to carbon nuclei, and the relaxation delay was set to 44.6 s to ensure ^{13}C complete relaxation. ^{1}H decoupling power was set to 0.2 W, and 2000 scans were accumulated using an acquisition time of 0.2 s. Deconvolution of the spectra, using BRUKER WIN 1D NMR software, provided the chemical shift of the resonance peaks of the two conformations, the corresponding half-line widths, and the ratio of the two populations. These data were used as initial values for the simulation of the peaks, using DNMR 7.1 software, in order to calculate the kinetic and thermodynamic parameters of the equilibrium between the two conformations.

2. Conformational Analysis. Molecular modeling analysis was performed on a Silicon Graphics O_2 workstation using QUANTA software (MSI) and CHARMm force field. Dielectric constant (ϵ) was set to 63 as an average of the

dielectric constants of DMSO ($\epsilon = 45$) and H_2O ($\epsilon = 81$) to simulate the mixture of solvents used in NMR studies. The first step in the conformational analysis of valsartan was to construct a preliminary 3D model which was minimized using the first order minimization algorithms, steepest descents, conjugate gradient, and Powell with 0.01 kcal.mol^{-1} as the convergence criterion. This conformer was further subjected to random sampling obtaining 1000 low energy conformers. Cluster analysis led to 11 clusters using a dihedral angle criterion. The lowest energy conformer of each cluster was further minimized. Among them, only two conformers satisfied the majority of the interatomic distances measured by the ROESY spectrum (ROEs) observed for major and minor conformations. These were assigned as initial major and minor conformers, respectively.

3. Docking Calculations. Molecular docking simulations using the FlexX algorithm of SYBYL[39] have been employed to the lowest energy conformers of valsartan obtained by a combination of experimental and molecular modeling results. FlexX uses a fast docking method that allows flexibility in the ligands, keeping the receptor rigid, and it uses an incremental construction algorithm in order to place flexible ligands into a fully specified binding site. The default FlexX scoring function was used in the calculations. FlexX uses formal charges, which were turned on during docking.

In order to examine the effect of *sn*−2 dipalmitoyl phosphatidylcholine (DPPC) bilayers on the docking calculations, two different docking simulations of valsartan have been performed: (i) to the homology model of the AT1 receptor and (ii) to the receptor site in the presence of DPPC bilayers. The 3D model of the AT1 receptor used was constructed and kindly provided to us by Tuccinardi et al.[40] with a molecular modeling procedure, using the X-ray structure of bovine rhodopsin[41] as the initial template and taken into account the available site-directed mutagenesis data. The active site in the docking runs included all atoms within a radius of 2.0 Å around the critical amino acids: VAL108, LEU112, TYR113, ALA159, VAL179, ALA181, PHE182. TYR184, LYS199, ASN200, LEU202, GLY203, TRP253, HIS256, GLN257, MET284, ILE288.

4. MD Simulations. MD simulations have been performed on two systems in order to examine the stability of the ligand inside the binding pocket and optimize the binding interactions between receptor and ligand: (a) explicitly solvated AT1 receptor with valsartan at the binding site and (b) AT1 with valsartan at the binding site of the receptor surrounded by a DPPC lipid bilayer environment and solvent molecules. Input coordinates of the valsartan/AT1 receptor complex for both (a) and (b) systems have been obtained from the corresponding highest ranked docked receptor−ligand pose of the docking calculations in which the valsartan adopts a *trans* (major) conformation. System (a) includes the valsartan ligand, the AT1 receptor, and 33379 water molecules in a cubic box with dimensions 101.8 (Å)^3. System (b) includes the ligand, the AT1 receptor, and the DPPC lipid bilayer obtained from Dr. M. Karttunen's Web page[42] (128 DPPC lipids and 3655 water molecules after 100 ns MD simulation.[43,44] The lipid was extended by 4 × 4 × 1 in xyz axes in order to have enough area of lipid for the protein merging.). For comparative reasons we have selected aqueous and lipid bilayer environments. An aqueous environment is commonly used for MD simulation studies.[21,45] The MD simulations

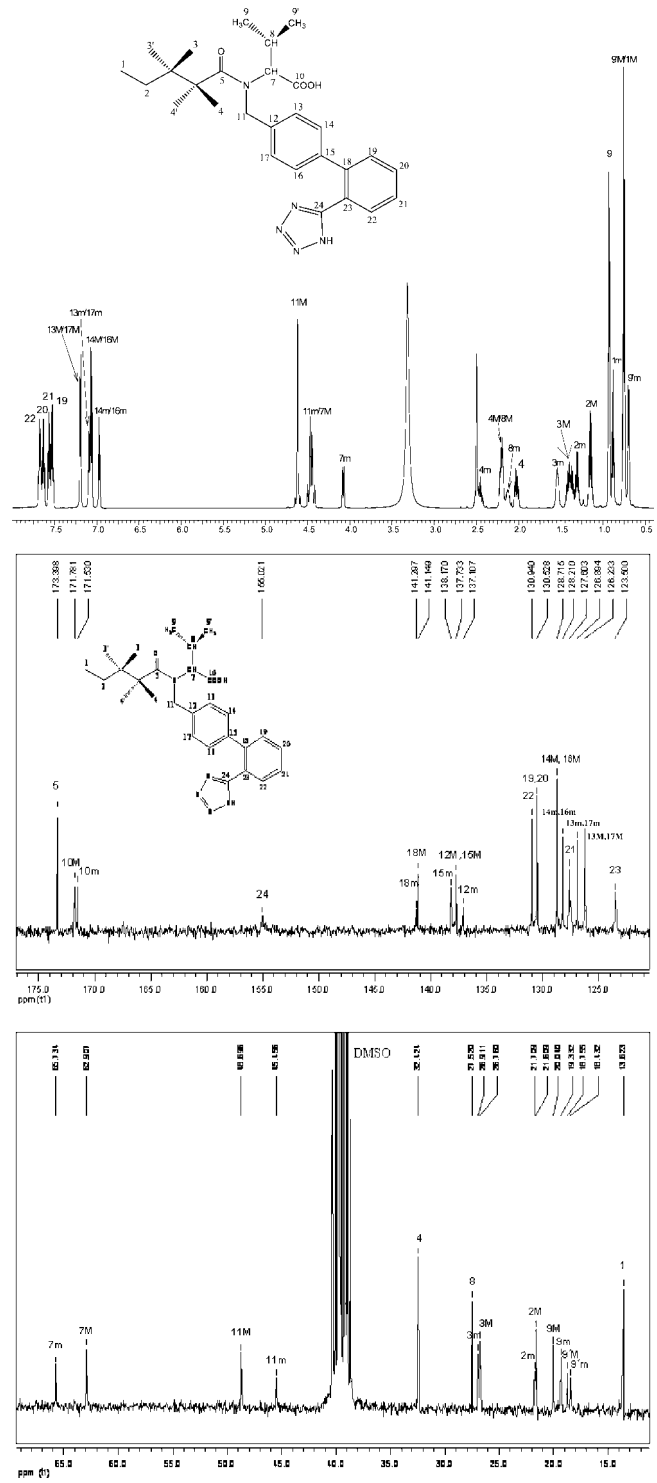

Figure 2. (top) ^{1}H NMR spectrum of valsartan obtained at 27 °C in DMSO-d_6 solvent. M and m represent the major and the minor conformations, respectively. (bottom) ^{13}C NMR spectrum of valsartan was obtained at 27 °C.

were performed with GROMACS 3.3.1 software package[46] using the GROMOS96 force field.[47] Simulations were run in the NPT ensemble at 300 K and 1 bar with periodic boundary conditions. During equilibration the Berendsen barostat and thermostat algorithms[48] were applied. Electrostatic interactions were calculated using the particle mesh Ewald method.[49] Cutoff distances for the calculation of Coulomb and van der Waals interactions were 1.0 and 1.4 nm, respectively. Prior to the dynamics simulations, energy minimization was applied to the full system without con-

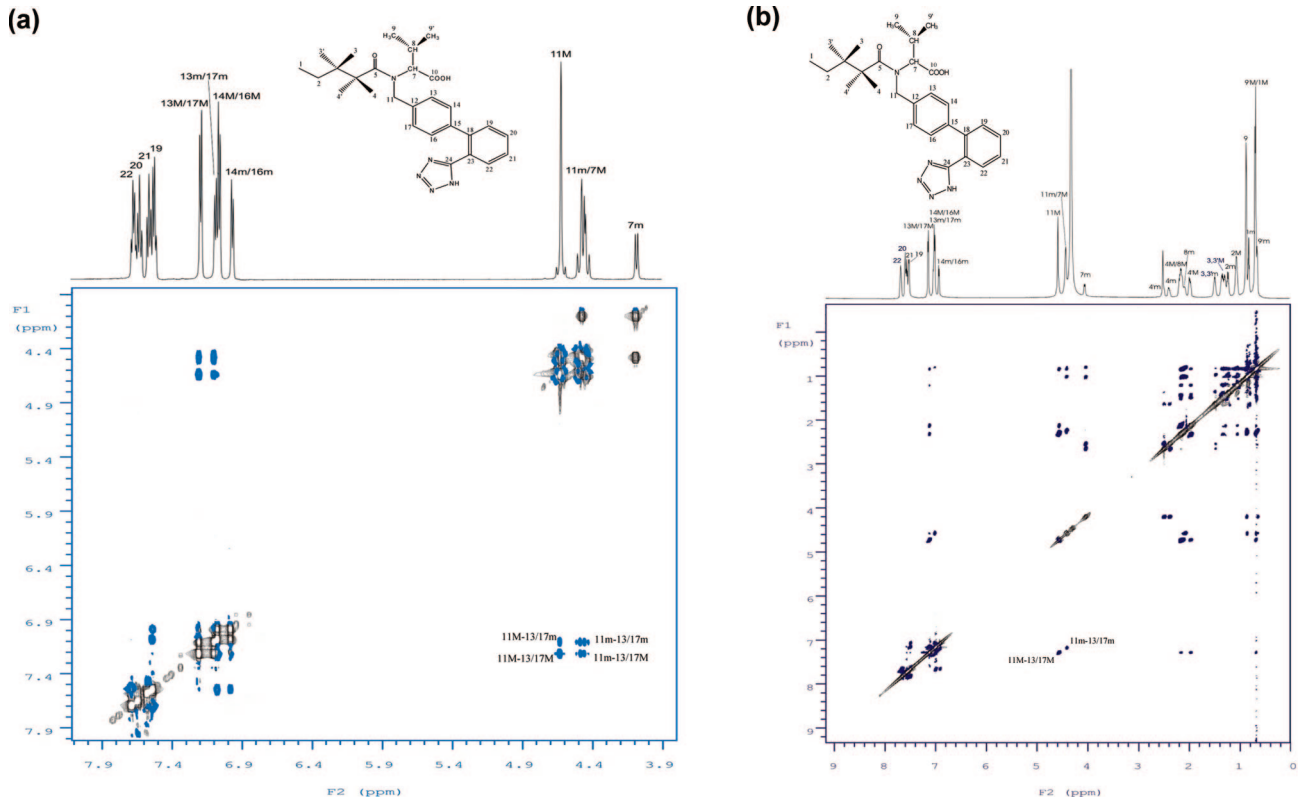

Figure 3. a. 2D ROESY spectrum of valsartan obtained in DMSO-d_6 at 300 K (region 3.9−8.0 ppm). b. 2D ROESY spectrum of valsartan obtained in DMSO-d_6/D_2O at 273 K.

straints using the steepest descent integrator for 2000 steps with the initial step size of 0.01 Å (the minimization tolerance was set to 1000 kJ/(mol.nm)). The systems were then equilibrated via 250 ps simulations with a time step of 2 fs. Finally, a 2 ns and 2.5 ns production run was performed for systems (a) and (b), respectively, at 300 K and 1 bar with a time step of 2 fs using Berendsen thermostat and Parrinello-Rahman barostat[50] algorithms. All bonds were constrained using the LINCS algorithm.[51] Visualization of the dynamics trajectories was performed with the VMD software package.[52] The Origin 6.0 program[53] was used for the plots.

5. Quantum Mechanics and ONIOM Calculations. The barrier for rotation around the critical valsartan τ_6 torsion angle (Figure 1) was also calculated theoretically using quantum mechanics (QM) and the ONIOM[54] method. Specifically, QM calculations using DFT were performed on a simplified model valsartan with the groups at positions 8 and 11, and the alkyl chain attached to C5 replaced by methyl groups (Figure 1). The B3LYP method[55] was used together with the 6−31G* basis set[56] for optimization and location of stationary points in the gas phase, while single point energy (SPE) calculations at the optimum geometries were then performed using the larger aug-cc-pVDZ basis set[56] and the PCM continuum method[57] to account for solvation effects (H_2O). The rotational TS for the real valsartan molecule was calculated by optimizations using the ONIOM[57] method (B3LYP/6−31+G*: AM1) to include the full steric effects for τ_6 rotation, and these optimizations were also followed by SPE calculations in H_2O using the B3LYP/aug-cc-pVDZ + PCM method. The initial simplified valsartan model represented the QM part in the ONIOM calculations with the semiempirical AM1 method[58] accounting for the steric effects of the bulky valsartan substituents. Frequency calculations were performed on all optimized structures prior to the higher level of theory SPE calculations to fully characterize and validate the stationary points as minima or transition states for rotation with rotational transition states having one and only one imaginary frequency. Intrinsic Reaction Coordinate (IRC) calculations on the real valsartan molecule transition state were performed to help locate the connecting minimum stationary points. Computations were performed using Gaussian03.[59]

RESULTS AND DISCUSSION

1. Structure Assignment. Two distinct conformations of valsartan (Figure 1) are observed from ^1H and ^{13}C NMR spectra (Figure 2) due to the hindered rotation around its amide bond. The complete assignment of proton resonances of valsartan was achieved using 2D COSY (Supporting Information: Figures SF1 and SF2) and 2D ROESY spectra (Figure 3). Table 1 shows the ^1H and ^{13}C chemical shift assignments of valsartan in DMSO-d_6 solution at 300 K. For comparative purposes data obtained by Fang et al.[34] in CD_3OD are also reported. As can be observed from Table 1 the differences between the chemical shifts in the two environments are limited mainly to carbonyl and carboxylate carbons. In methanol solvent, enolization leads to increased positive charges on the resonated carbonyl and carboxylate carbons. Thus, carbons in the vicinity of the carbonyl or carboxylate are the most affected and deshielded (i.e, carbons designated with the numbers 2, 4, 5, 8, 11, 12, 15, and 18 have $\Delta\nu$ >2 ppm in the methanol environment). This enolization effect is also observable in ^1H NMR spectroscopy. Again protons in the vicinity of the amide bond are the most affected and deshielded (i.e protons designated with

Table 1. Comparison of ^{1}H and ^{13}C NMR Chemical Shifts (in ppm) of Valsartan in CD_3OD[34] and DMSO-d_6 Solutions

number	^{1}H Major[34] (CD_3OD)	^{1}H Major (DMSO-d_6)	$\Delta\nu$ (ppm)	^{13}C Major[34] (CD_3OD)	^{13}C Major (DMSO-d_6)	$\Delta\nu$ (ppm)
1	0.84	0.75	0.09	14.50	13.60	0.90
2	1.24	1.15	0.09	23.70	21.60	2.10
3	1.51	1.37, 1.39	0.14, 0.12	28.80	26.70	2.10
4	2.19, 2.33	2.04, 2.20	0.15, 1.13	34.80	32.40	2.40
5				177.50	173.40	4.10
7	4.58	4.45	0.13	65.20	62.90	2.30
8	2.31	2.21	0.10	29.60	27.50	2.10
9′	0.84	0.75	0.09	19.70	18.70	1.00
9	1.00	0.93	0.07	20.90	20.00	0.90
10				173.90	171.80	2.10
11	4.62, 4.80	4.62	0.00, 0.18	50.90	48.70	2.20
12				139.10	137.70	1.40
13	7.24	7.20	0.04	128.10	126.20	1.90
14	7.10	7.06	0.04	130.60	128.70	1.90
15				140.00	137.70	2.30
16	7.10	7.06	0.04	130.60	128.70	1.90
17	7.24	7.20	0.04	128.10	126.20	1.90
18				143.40	141.10	2.30
19	7.55	7.53	0.02	132.10	130.50	1.60
20	7.67	7.63	0.04	131.90	130.50	1.40
21	7.56	7.57	−0.01	129.30	127.60	1.70
22	7.65	7.68	−0.03	132.80	130.90	1.90
23				124.70	123.50	1.20
24				156.90	155.00	1.90

number	^{1}H Minor[34] (CD_3OD)	^{1}H Minor (DMSO-d_6)	$\Delta\nu$(ppm)	^{13}C Minor[14] (CD_3OD)	^{13}C Minor (DMSO-d_6)	$\Delta\nu$(ppm)
1	0.95	0.88	0.07	14.50	13.60	0.90
2	1.38	1.31	0.07	23.80	21.70	2.10
3	1.66	1.54	0.12	28.90	26.90	2.00
4	2.50, 2.64	2.46	0.04, 0.18	34.70	32.40	2.30
5				177.30	173.40	3.90
7	4.14	4.08	0.06	68.20	65.70	2.50
8	2.24	2.13	0.11	29.50	27.50	2.00
9′	0.79	0.70	0.09	19.60	18.40	1.20
9	1.01	0.93	0.08	20.30	19.30	1.00
10				173.30	171.50	1.80
11	4.60	4.47	0.13	47.60	45.50	2.10
12				139.80	137.10	2.70
13	7.18	7.09	0.09	129.00	126.90	2.10
14	7.02	6.97	0.05	130.10	128.20	1.90
15				139.10	138.20	0.90
16	7.02	6.97	0.05	130.10	128.20	1.90
17	7.18	7.09	0.09	129.00	126.90	2.10
18				143.60	141.30	2.30
19	7.53	7.53	0.00	132.10	130.50	1.60
20	7.66	7.63	0.03	132.80	130.50	2.30
21	7.54	7.57	−0.03	129.20	127.60	1.60
22	7.64	7.68	−0.04	132.00	130.90	1.10
23				124.50	123.50	1.00
24				157.00	155.00	2.00

the numbers 3, 4, 7, 8, and 11 have $\Delta\nu$ >0.10 ppm in the methanol environment).

2. 2D-NMR ROESY Spectroscopy. 2D ROESY spectra show two kinds of off diagonal peaks: those which correspond to the exchanging nuclei between the two conformations being in the same phase with the diagonal and those which have an opposite phase relative to the diagonal are attributed to NOE interactions.

The presence of exchange signals between the two observed conformations is eminent at room temperature which diminishes when lowering the temperature. This effect can be visualized in Figure 3a where protons H-11 of the major conformation show ROE signals with protons H-13/17 of both major and minor conformation. In order to overcome this problem. 2D ROESY experiment was run at 273 K where the exchange process between the two conformations is slow on the NMR time scale (Figure 3b). At this temperature a mixture of solvents (DMSO-d_6/D_2O) 1:1 was used. The through space dipolar-dipolar correlations provide important information on molecule conformations since their magnitudes are inversely proportional to the sixth power of the interproton distance. The most important observed ROEs for each conformation and the derived distances after quantification of the off diagonal signals are shown in Table 2.

The ROEs of the major conformation between the protons H4M-H13/17M, H4′M-H13/17M, H4M-H11M, and H4′M-H11 M establish the vicinity between the *n*-butyl chain and the biphenyl ring.

Three critical ROEs are observed in the minor conformation. The signal between protons H8m-H11m indicates the vicinity of the isopropyl group with the spacer methylene

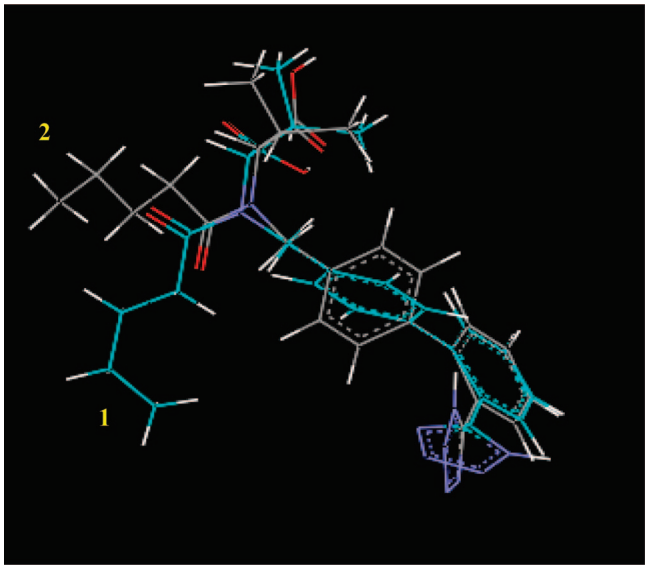

Figure 4. Low energy conformers **1** (dihedral angles $\tau_1 = 142.4$, $\tau_2 = -49.0$, $\tau_3 = -98.0$, $\tau_4 = 79.2$, $\tau_5 = -121.2$, $\tau_6 = 165.4$, $\tau_7 = -134.5$, $\tau_8 = 69.7$, $\tau_9 = -153.2$, $\tau_{10} = 81.0$, $\tau_{11} = -3.6$) and **2** (dihedral angles $\tau_1 = 39.0$, $\tau_2 = 45.3$, $\tau_3 = 81.1$, $\tau_4 = -120.4$, $\tau_5 = 67.6$, $\tau_6 = 2.3$, $\tau_7 = -104.7$, $\tau_8 = -87.3$, $\tau_9 = 174.6$, $\tau_{10} = -179.5$, $\tau_{11} = -179.9$) of valsartan derived using energy minimization algorithms and random sampling conformational search method. These low energy conformers satisfy the critical ROEs determining the minor and major conformation respectively and are used as initial structures for docking experiments.

Table 2. Interproton Distances for Each Conformation of Valsartan[a]

valsartan major		valsartan minor	
protons	distance (Å)	protons	distance (Å)
H19M-H14/16M	2.28	H19m-H14/16m	2.15
H11M-H13/17M	2.34	H11m-H13/17m	2.33
H9′M-H13/17M	3.74	H9′m-H13/17m	3.85
H9M-H7M	3.17	H9m-H7m	2.50
H9′M-H7M	3.25	H9′m-H7m	2.69
H9′M-H11M	2.96	H9′m-H11m	3.27
H4M-H13/17M	2.92	H8m-H11m	2.08
H4′M-H13/17M	2.68	H4′m-H7m	1.85
H4′M-H11M	2.41	H4m-H7m	1.89
H4M-H11M	1.84	H1m-H3.3′m	3.02

[a] The exclusive ROEs for the major conformation are underlined in the valsartan major column and the ones of minor conformation in the valsartan minor column.

group attached to the biphenyltetrazole group. The other two ROEs between protons H4m-H7m and H4′m-H7m show the proximity of the butyl chain methylene adjacent to the amide bond with the α-CH of the carboxyl group.

3. Conformational Search Results. The conformational space of valsartan was explored using energy minimization and random sampling algorithms. Among the low energy conformers derived, only conformers **1** and **2** (Figure 4) are the ones which satisfied the critical ROEs determining the minor and major conformation, respectively. These conformers were used as input structures for docking calculations.

4. *In Silico* Docking Results. Figure 5 shows the highest docked structure of valsartan at the active site of the receptor. The best binding score was obtained as −15.72 kJ/mol. Three hydrogen bonds (using a distance cutoff of 3.5 Å and an angle cutoff of 30°) are observed between active site residues and the ligand. More specifically these hydrogen bonds were

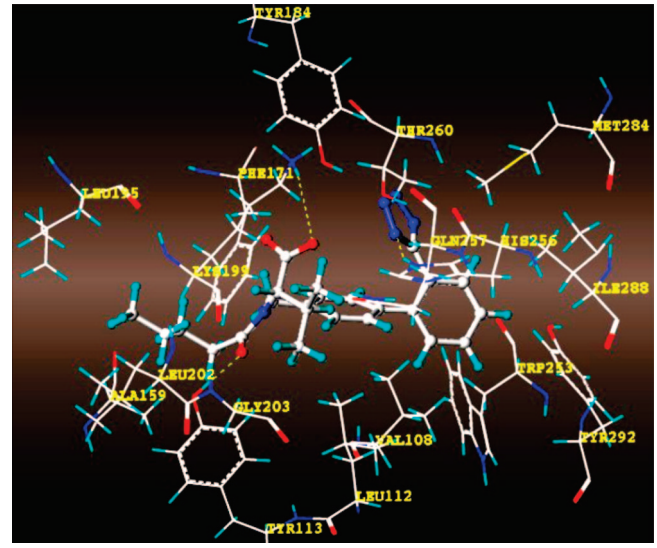

Figure 5. The top ranked docking pose of valsartan at the active site of the AT1 receptor.

observed between a LYS199 side chain amine hydrogen and a ligand carboxylate oxygen, between a backbone amine H of HIS256 and the ligand tetrazole group, and between the phenolic hydrogen atom of TYR113 and the ligand carbonyl oxygen (Figure 5). The incorporation of the lipid bilayer in the docking calculations at the active site of the receptor did not show a significant effect on the binding score as it was expected. It should be mentioned that only 10% of the highest generated poses of valsartan adopted the *cis* (minor) conformation.

5. MD Simulations. Figure SF7 in the Supporting Information shows a snapshot of systems used in the MD simulations. Superimposition of representative AT1 receptor/valsartan complexes after MD simulations in two different environments has been shown in Figure 6 (top), in order to show how AT1/valsartan complexes differ in water and lipid bilayer membrane models. Atom positions between the representative receptor models derived from bulk water and membrane bilayer medium simulations have been shown with a color scale model, more clearly in Figure 6 (bottom). For this purpose, a script with a color scale has been used under the VMD program where blue colored places show no change in distance and red colored places show highly flexible regions (if change of the distances based on α carbons are more than 4 Å). As it is clearly shown in the figure, there is an important change in conformation at the binding site of the receptor in two different simulations. Receptor amino acid residues in a lipid environment are in a closer spatial vicinity than in a bulk water environment (Figure 6). The trajectory analysis results are shown in Figure 7 for both systems on the alkyl side chain of the ligand. The results have shown that τ_6 and τ_9 torsion angles adopt values of ∼160° and ∼220°, respectively, with small perturbations around these values for a ligand at the active site of the receptor system, and these values are slightly altered to ∼140° and ∼240° when the system is surrounded by the bilayer. Dihedral angles τ_{10} and τ_{11} are more flexible than the others and form both *trans* and *gauche* conformations for both of the MD systems (torsion angles are defined in Figure 1).

The MD simulations results revealed that during the simulations binding between active site residues and ligand becomes optimized with respect to hydrogen bonds compared to the

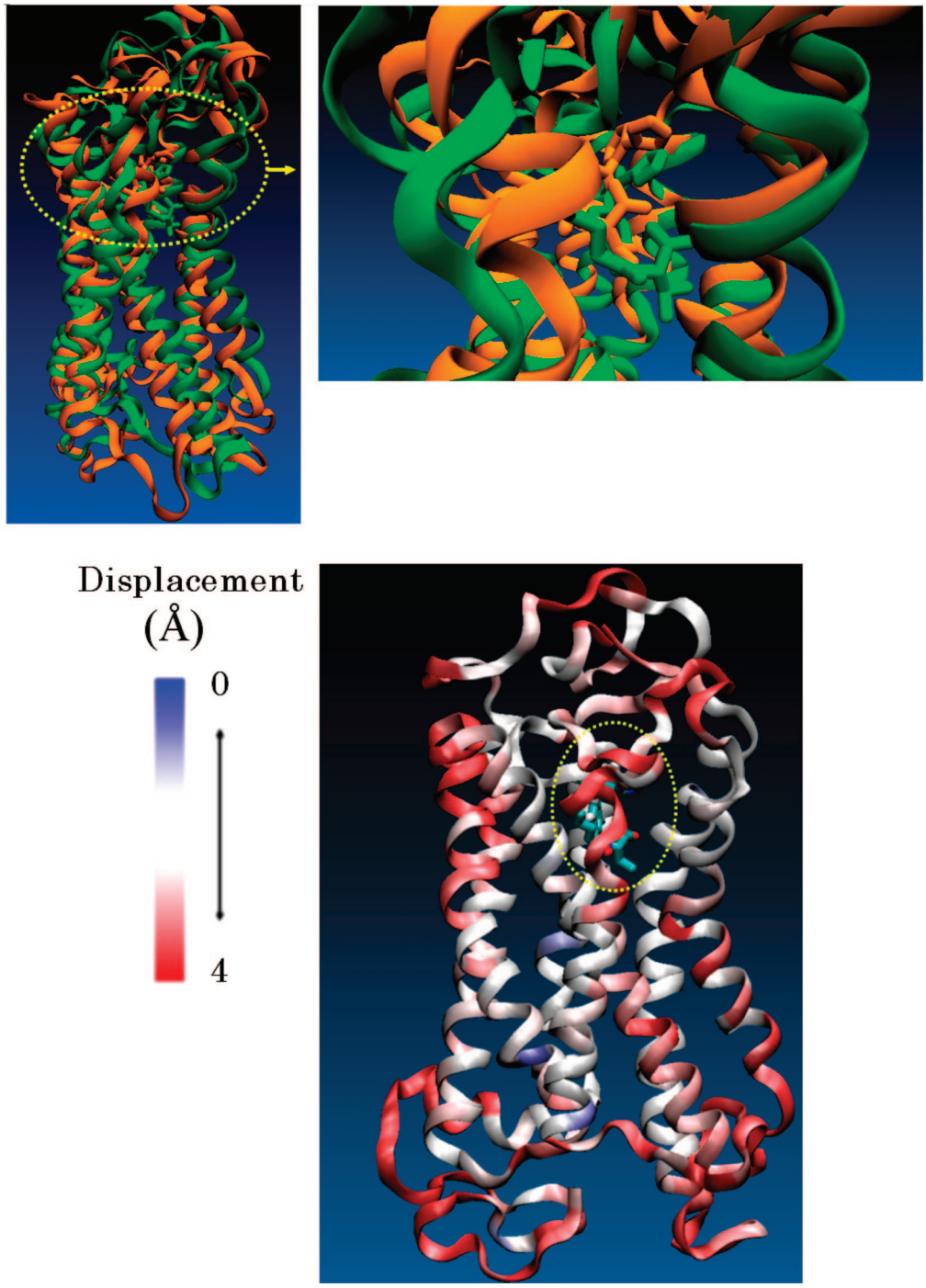

Figure 6. (top) Superimposition of representative AT1/valsartan complexes after MD simulations in two different environments (green colored) helices, explicitly solvated AT1 receptor/valsartan complex; (orange colored) helices, AT1/valsartan complex surrounded by a DPPC lipid bilayer and solvent molecules. (bottom) Atom positions between the representative receptor models derived from bulk water and membrane bilayer medium simulations have been shown with a color scale model. Blue colored fields show no change in displacement; red colored fields show high flexible regions.

docking results. Docking calculations have shown that active site residue LYS199 forms only one hydrogen bond with the carboxylate oxygen of the ligand. MD results have shown that the flexible residue LYS199 can locate itself between carboxylate and tetrazole groups of the ligand in order to form multiple hydrogen bonds. When the DPPC bilayer is included in the system, valsartan shows better packing (Figure 8, top). Hydrogen bonds are formed between the side chain amine hydrogens of LYS199 and both the oxygen atoms of carboxylate and the nitrogen atoms of the tetrazole group of the ligand; between PHE182, TYR184, and THR260 amino acids and the tetrazole group of the ligand; between GLN257 and the carboxylate group of the ligand; and between SER109 and the C═O group of the ligand. The average number of hydrogen bonds throughout the simulations increases from 8.45 to 10.09 when simulations are carried out including the lipid bilayer (Figure 8, bottom).

MD simulations results for both systems confirm that at the active site of the receptor the tetrazole and the carboxylate groups of ligand must be close to each other to form multiple hydrogen bonds with flexible amino acid residue LYS199. Figure 9 shows the superimposition of the conformations of

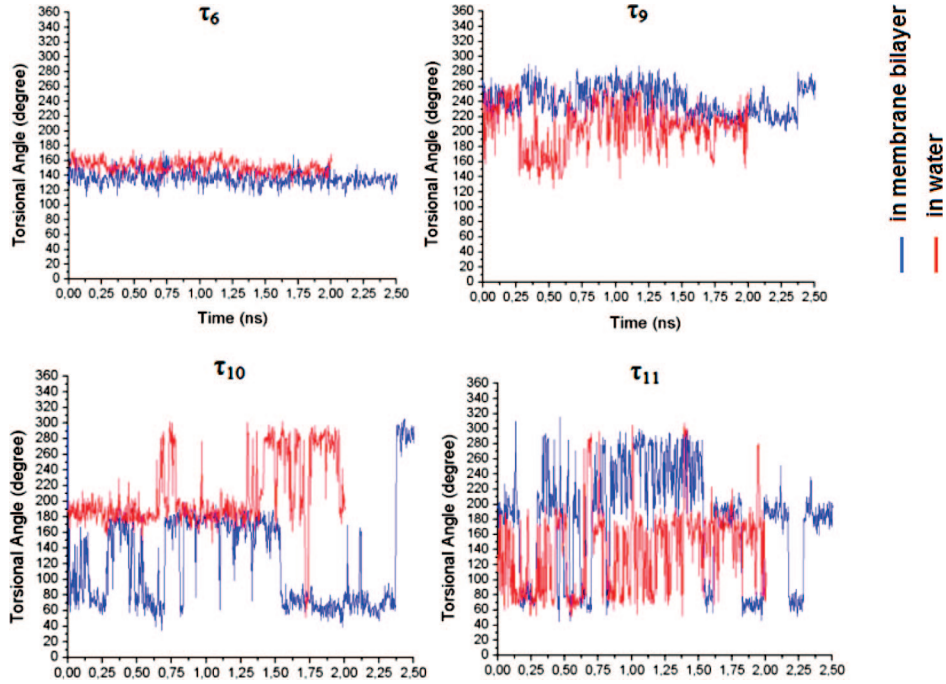

Figure 7. Fluctuations of dihedral angles τ_6 and $\tau_9-\tau_{11}$ torsional angles (defined in Figure 1) in the MD simulations for the system of the ligand at the binding site of the AT1 receptor without the lipid bilayer (shown with red color) compared to surrounded by the lipid bilayer (shown with blue color). Because of the different number of atoms for two simulations, simulation time was longer for the more complex system containing the lipid bilayer.

valsartan that form the highest number of hydrogen bonds throughout the MD simulations.

6. Dynamic NMR Spectroscopy. In order to provide more information regarding the kinetic and thermodynamic parameters of the equilibrium between the two conformations, dynamic NMR experiments were performed.

The temperature dependence of the exchange phenomenon of valsartan can be visualized in Figure 10 where the ^{1}H NMR spectral region 0.30−1.85 ppm is depicted for the temperature range of 35 to 70 °C with 5 °C intervals. The temperature increase is accompanied by broadening of the resonance peaks corresponding to the two distinct conformations. Coalescence of the peaks is observed around 60 °C, while above this temperature the system undergoes fast exchange resulting in one peak resonating at the weighted average of the resonance frequencies of the two component peaks.

The two conformations of valsartan exist in a dynamic equilibrium as shown below:

$$major \underset{k_{-1}}{\overset{k_1}{\rightleftarrows}} minor$$

The kinetic and thermodynamic parameters of the dynamic equilibrium were estimated using two different approaches: (i) application of 2D EXSY NMR and (ii) ^{13}C NMR line shape analysis.

(i) Application of 2D EXSY NMR. The region 1.0−2.9 ppm was selected for the calculation of the rate constants since the least overlapping of the resonance peaks occurs at this region. Particularly, the diagonal and cross peaks signals of the following proton pairs are measured: 2M-2m, 3,3′M-3,3′m, and 4′M-4′m (Figure 11). For each mixing time, the mean values of k_1 and k_{-1} are calculated using the measured intensities. Subsequently, these values are used to estimate the average value of the constant rates generated. Having determined the constant rates of k_1 and k_{-1}, the activation Gibbs free energy for each interconversion is calculated from the following equation[36]

$$\Delta G^{\#} = -RT\ln\frac{kh}{k_B T} \quad (1)$$

where R is the gas constant, h is Planck's constant, k_B is the Boltzmann constant, T is the temperature (K), and k is the rate constant of exchange (s^{-1}).

$\Delta G^{\#}_1$ values correspond to the conversion from the major to the minor conformation and $\Delta G^{\#}_{-1}$ correspond to the opposite conversion. The standard deviation is calculated using eq 2:

$$\sigma(\Delta G^{\#}) = RT\left[\left(\frac{\Delta k}{k}\right)^2 + \left(1 - \ln\frac{kh}{k_B T}\right)^2\left(\frac{\Delta T}{T}\right)^2\right]^{1/2} \quad (2)$$

The temperature variation was $\Delta T = 0.1$ K.

(ii) ^{13}C NMR Line Shape Analysis. Dynamic NMR line shape analysis was applied to ^{13}C spectra, due to the wider dispersion and less overlapping of the resonance peaks compared with ^{1}H NMR spectra. ^{13}C quantitative NMR experiments were run at the temperature range of 20−70 °C. Figure 2 depicts the spectrum acquired at 27 °C where aliphatic and aromatic regions are separated. Assignment of the peaks was enabled by the use of 2D-HSQC and 2D-HMBC NMR experiments (Supporting Information: Figures SF3−SF5). For the subsequent analysis, the least overlapped resonance peaks corresponding to the two conformations were selected, namely peaks 9M-9m, 11M-11m, 7M-7m, (13/17)M-(13/17)m, and (14/16)M-(14/16)m. A representative ^{13}C NMR spectral region (13−23 ppm) including peaks 9M-9m is illustrated in Figure SF6 of the Supporting Information for the temperature range

of 20 to 70 °C. As observed, the coalescence occurs in a temperature range of 55−60 °C.

Deconvolution of the above selected resonance peaks provided: i) the chemical shift; ii) the corresponding half-line widths; and iii) the ratio of the two populations (p_m/p_M), in all studied temperatures. The derived data were used for line shape analysis simulation in order to calculate the rate constants and the thermodynamic parameters of the interconversion. Gibbs free energies of activation $\Delta G^{\#}_1$ and $\Delta G^{\#}_{-1}$ and the associate standard deviations were again calculated using eqs 1 and 2. Furthermore, Gibbs free energy of the equilibrium ΔG^0 was estimated using formula 3.

(iii) Thermodynamic Parameters. Comparative equilibrium constants K_{eq} values for temperature range 293−303 K for valsartan are obtained using the exchanging protons H-2 and H-3. K_{eq} values for H-16 and H-17 could not be obtained due to the fact that the peaks of the minor conformer attributed to H13 and H17 were overlapping with those of the major peak attributed to H-14 and H-16. K_{eq} values of H-4 could be obtained and are not reported by Fang et al.[34] The mean K_{eq} values, reported by Fang et al.,[34] are taking into account H-2, H-3, H-16, and H-17 and are compared with those obtained by us using H-2, H-3, and H-4 protons. Mean K_{eq} values were found to be identical for 293 K and equal to 0.58. The mean K_{eq} value at 303 K was found to be 0.58 by Fang et al.[34] and 0.59 in our studies. As it can be seen the obtained equilibrium constants by these two different studies were almost identical, indicating that solvent does affect the equilibrium constant.

$$\Delta G^0 = -RT \ln K_{eq} = -RT \ln\left(\frac{n_m}{n_M}\right) = -RT \ln\left(\frac{p_m}{p_M}\right) \quad (3)$$

$\Delta G°$ values for the two laboratories were also of similar magnitude: 0.32 ± 0.04 kcal/mol values were found by Fang et al.[34] and 0.19 ± 0.05 kcal/mol at 20 °C to 0.22 ± 0.02 kcal/mol at 70 °C were found in our studies showing that $\Delta G°$ in the DMSO solvent was lower than that observed in CD_3OD.

(iv) Kinetic Parameters. The activation enthalpy ($\Delta H^{\#}$) by Fang et al.[34] was found to be 17.9 ± 0.7 kcal/mol, while in our studies the energy barrier ($\Delta G^{\#}_1$) for the transition from the major to the minor conformation ranged between

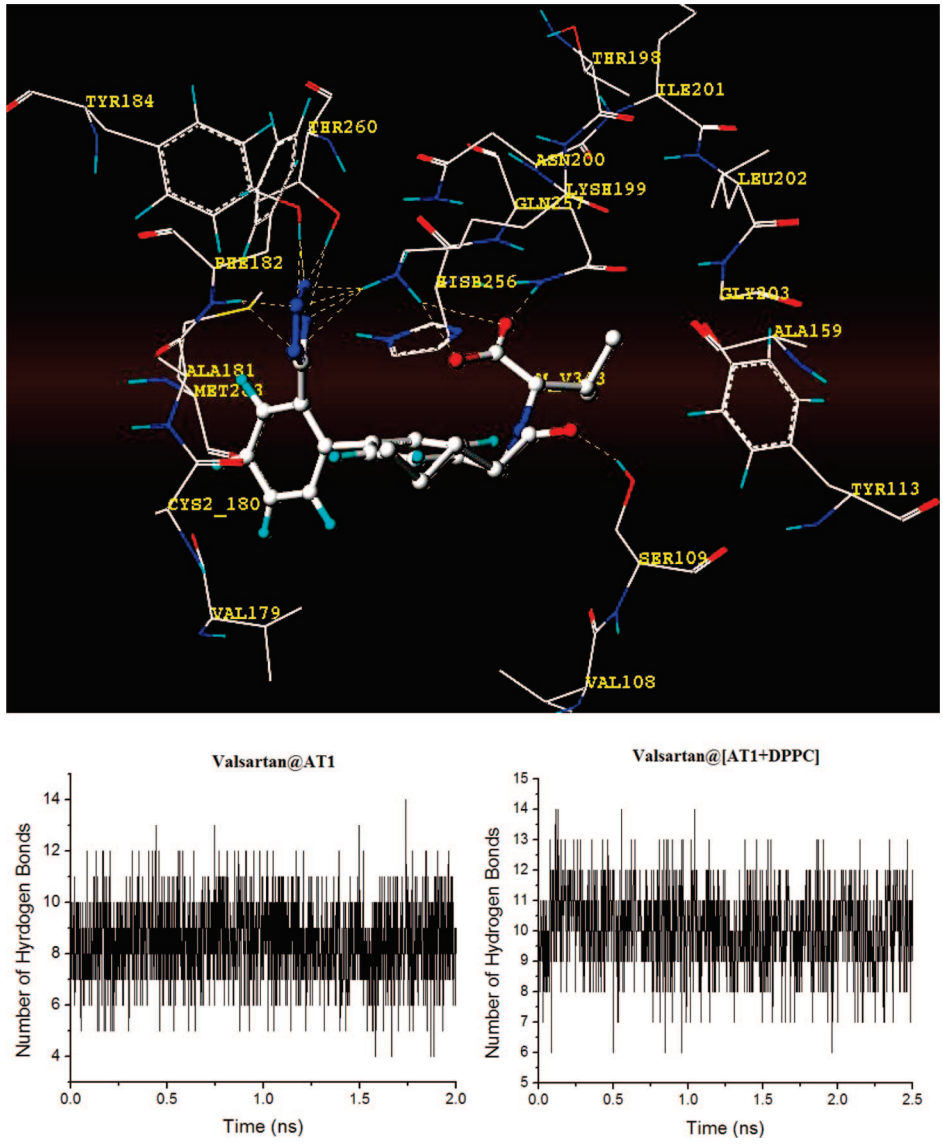

Figure 8. (top) Formed hydrogen bonds throughout the simulation of ligand at the active site of the receptor surrounded with lipid bilayer system. (bottom) The number of hydrogen bonds throughout the simulations (left) ligand at the binding site of the AT1 receptor (right) ligand at the binding site of the receptor surrounded by lipid bilayer.

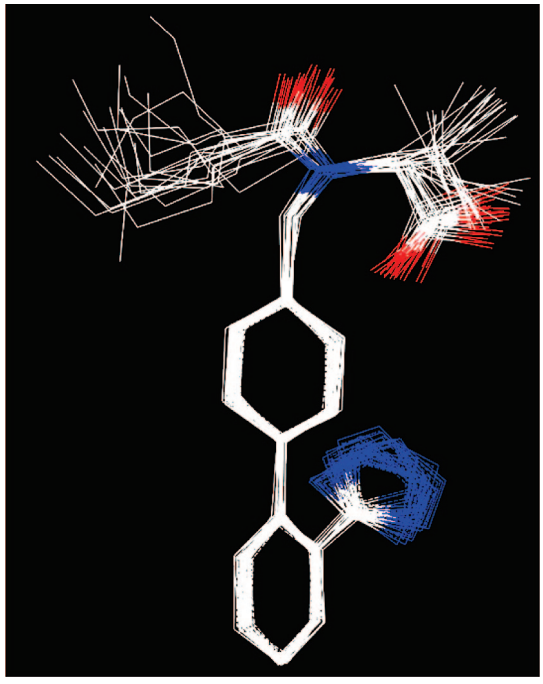

Figure 9. Superimposition of snapshots of conformations of ligand that form the highest number of hydrogen bonds throughout the simulation.

16.78 ± 0.14 kcal/mol and 17.49 ± 0.04 kcal/mol and the inverse transition energy barrier ($\Delta G^{\#}_{-1}$) ranged between 16.61 ± 0.08 kcal/mol to 17.08 ± 0.07 kcal/mol. The energy difference ΔG^0 between the two conformations in equilibrium is therefore very small compared to the energy barriers for interconversion. The Gibbs free energies of activation $\Delta G^{\#}_1$ and $\Delta G^{\#}_{-1}$ deduced by both methods are in a good agreement. Furthermore, it is observed that $\Delta G^{\#}_1$ is higher than $\Delta G^{\#}_{-1}$ at each temperature, in accordance with the higher propensity observed for the major conformation.

Results obtained from both methodologies yield a conversion rate from the minor to the major conformation almost twice that for the opposite conversion. Thus, the population ratio remains practically constant at the temperature range of 20−60 °C and equals to 3:2 (major:minor).

7. QM and ONIOM Calculation Results. The results of the dynamic NMR studies were further corroborated by calculation of the barriers for rotation using Gaussian03.[59] Full QM optimizations using DFT (B3LYP/g-31G*) were performed to calculate the rotational transition state around the critical valsartan τ_6 torsion angle (Figure 1) for a simplified model system in the gas phase, followed by a higher level of theory SPE calculations at the optimum geometries using B3LYP/aug-cc-pVDZ + PCM to account for the solvation effects (H_2O). The results of these high level preliminary calculations produced $\Delta G^{\#}_1$ and $\Delta G^{\#}_{-1}$ barriers for rotation of 23.1 kcal/mol connecting almost equally stable *cis* and *trans* conformations. The stationary points for rotation in the real valsartan molecule (Figure 12) were then calculated using the ONIOM method (B3LYP/6−31+G*: AM1) to include the full steric effects, and these optimizations were also followed by a higher level of theory SPE calculations in H_2O (B3LYP/aug-cc-pVDZ + PCM) to get more accurate energies. The results of these high level SPE calculations revealed lower barriers for rotation compared to the model valsartan. The barriers from trans ($\Delta G^{\#}_1$) and cis ($\Delta G^{\#}_{-1}$) conformers were calculated to be 17.1 kcal mol^{-1} and 18.0 kcal mol^{-1} at this level of theory, respectively, in very good agreement with experiment (although with a slight preference for a cis instead of a trans conformer). On inspection of the transition state (Figure 12), the lower barrier in the real valsartan system can be accounted for by three types of stabilization of the rotational transition state (τ_6 = −54.7°): (a) CH-π interactions between H4 (or H4′) and ring A which are accentuated on observing the transition state vibrational mode; (b) stabilization of rotating amide carbonyl O by six CH interactions (<2.9 Å and shown in Figure 12) with the bulky valsartan groups [CHs at positions 2, 3, 8, 9, 11, and 13(17)]; and (c) CH to

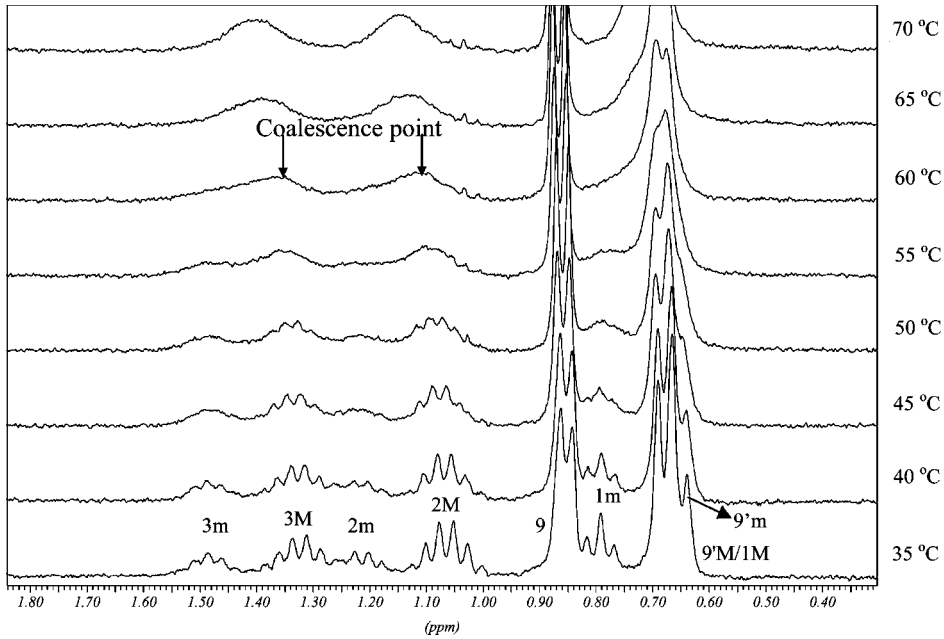

Figure 10. Spectral region (0.30−1.85 ppm) of ^{1}H (300 MHz) spectrum obtained at the temperature range of 35 to 70 °C.

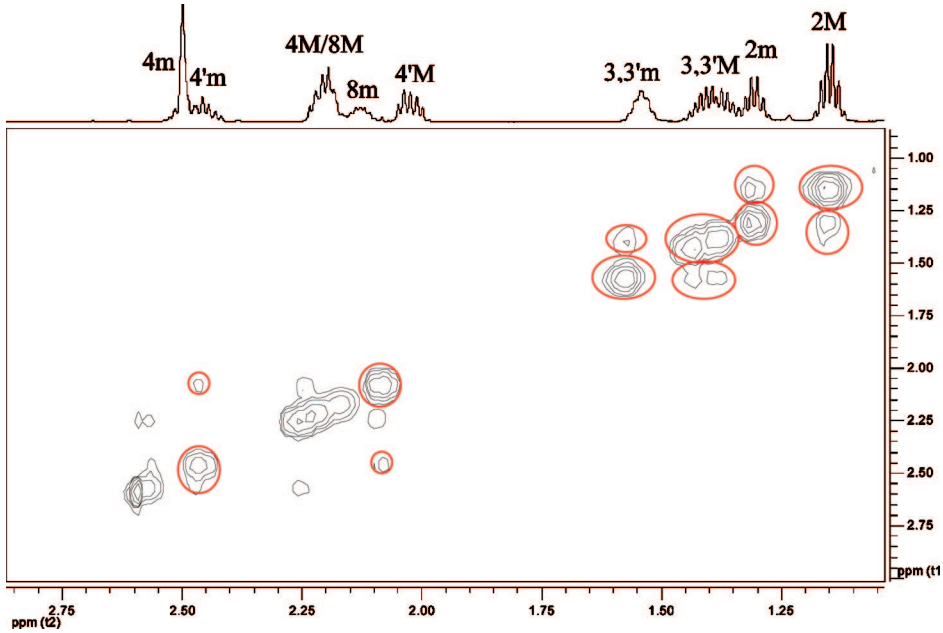

Figure 11. Spectral regions (1−2.9 ppm) of EXSY experiments obtained in DMSO-d_6 using mixing time t_m= 100 ms at 20 °C. The integration limits are symbolized with red curved lines.

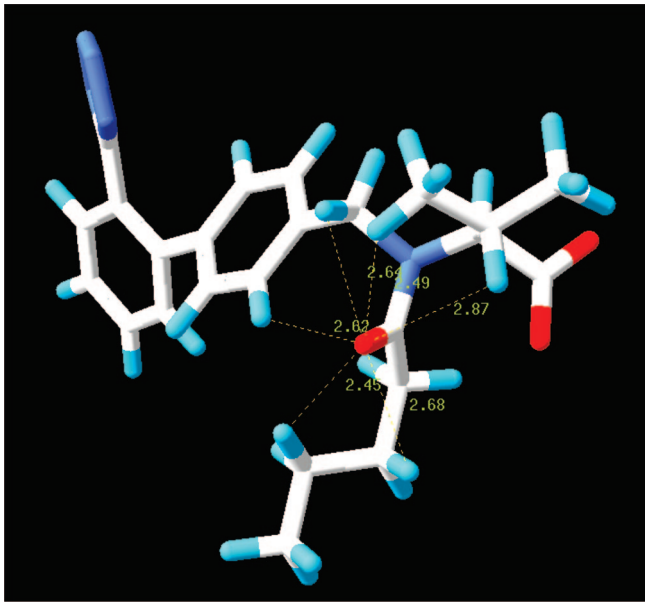

Figure 12. Conformation of valsartan rotational transition state as calculated using the ONIOM method. The stabilization of the amide carbonyl O by the surrounding CHs is explicitly indicated.

carboxylate O interactions resulting in a pseudo-chair-like 6 membered ring structure formed by N6, C5, C4, H4, O10, and C7.

CONCLUSIONS

The conformational properties of AT_1 antagonist valsartan in solution were elucidated using a combination of NMR spectroscopy and molecular modeling techniques. Two distinct conformations were observed in dynamic equilibrium with a constant population ratio at the temperature range of 20−60 °C.

The conformational differences between the observed conformers were localized mainly at the amide bond and the dihedral angles around it. The ratio between major:minor conformations was estimated to be 3:2. The two distinct conformations coalesce at the temperature range of 55−60 °C as it is depicted using ^{1}H and ^{13}C 1D NMR spectroscopy. QM and ONIOM calculations have revealed that the rotational TS between conformers is actually stabilized by the bulky valsartan groups.

In order to investigate the kinetic and thermodynamic parameters of the equilibrium, 2D EXSY-NMR as well as 1D ^{13}C NMR followed by line shape analysis were applied. Both approaches gave comparable results, revealing that the rate constant of the conversion from the minor to the major conformation is 2-fold compared to the opposite one. In the studied temperature range, the energy barrier ($\Delta G^{\#}_1$) for the transition from the major to the minor conformation ranged between 16.78 ± 0.14 to 17.49 ± 0.04 kcal/mol, while the inverse transition energy barrier ($\Delta G^{\#}_{-1}$) was estimated to range between 16.61 ± 0.08 to 17.08 ± 0.07 kcal/mol. As expected, $\Delta G^{\#}_1$ is slightly higher than $\Delta G^{\#}_{-1}$ for the examined temperature range. The two distinct conformations do not present a notable energy difference as implied by the Gibbs free energy of the equilibrium (ΔG^0) which was found to range between 0.19 ± 0.05 to 0.27 ± 0.08 kcal/mol.

The initial homology model of AT1 receptor used in our studies was the one developed by Tuccinardi et al.[28] However, some differences in the system of receptor and ligand are worth mentioning: (i) Docking and molecular dynamics (MD) simulations software are different for these two studies (in the presented study, FlexX docking and Gromacs MD programs have been used, while in the work by Tuccinardi et al., AutoDock and AMBER programs have been used, correspondingly). (ii) In the present study, MD simulations have been performed for a 2.5 ns simulation time, a longer simulation time than Tuccinardi's et al. work who used a 1 ns simulation time. (iii) Our docking studies have included DPPC bilayers in the system. (iv) Tuccinardi's et al. research work investigates the docking of several molecules of the sartans' group, while our research activity

focuses on the two conformers of valsartan, not mentioned in their study.

The model of the Tuccinardi et al. was treated as explained above and is consistent with mutation studies. In particular, valsartan interacted with amino acids Lys199, Gln257, and Ser109 which were found to be critical for the binding interactions in mutation studies.[60,61]

Docking experiments revealed that the highest affinity poses adopted by valsartan at the active site in the presence and absence of lipid bilayers have a ratio of approximately 9:1 major:minor conformations.

MD simulations shed more light on the mechanism of action of valsartan. LYS 199 was seen to form a bridge between the two acidic moieties of carboxylate and tetrazole. This allowed the acidic groups to form multiple hydrogen bonds. Thus, the system is further stabilized and valsartan is more packed in this system. In our previous work we proposed a two step mechanism of action for AT1 antagonists.[27] In the first step the AT1 antagonist is inserted in the bilayer core, and in the second step it is diffused at the active site of the lipid bilayers. Thus, we proposed that lipid bilayers must contribute significantly in the interaction of AT1 antagonists at the active site.[27] The obtained results confirm this hypothesis. Valsartan is interacting more productively in a lipid bilayer environment enlightening the role of membranes in the drug action. This stabilizing role of lipid bilayers may be of paramount biological importance for AT_1 antagonists to exert their biological action.

Abbreviations. RAS, Renin Angiotensin System; AII, Angiotensin II; ARB, Angiotensin II Receptor Blockers; ACE, Angiotensin Converting Enzyme; MEP, Molecular Electric Potential; MD, Molecular Dynamics; EXSY, Exchange Spectroscopy; QM, Quantum Mechanics.

ACKNOWLEDGMENT

We wish to express our deep acknowledgment to Novartis for providing us valsartan and the State Scholarship's Foundation (IKY) of Greece for financially supporting Dr. P. Zoumpoulakis. This research activity was also by GSRT (EPAN, HERCULES) and bilateral collaboration funding between Slovenia-Cyprus BI-CY/08-09-004 (2008−2009) from the Research Promotion Foundation (RPF) of Cyprus and the Slovenian Research Agency. Serdar Durdagi was funded by the European Union within the sixth Framework programme-Marie Curie Actions (Project: EURODESY-MEST-CT-2005-020575), while Joseph M. Hayes was funded by a Marie Curie Host Fellowship for the Transfer of Knowledge (ToK) contract no. MTKD-CT-2006-042776.

Note Added after ASAP Publication. This article was released ASAP on March 3, 2009 with the following errors: DMSO was changed to DMSO-d_6 and changes were made to the Acknowledgment. The correct version was posted on March 6, 2009.

Supporting Information Available: DQF-COSY spectral region (0−5 ppm) of valsartan at 27 °C (Figure SF1); DQF-COSY spectral region (6.5−7.8 ppm) of valsartan at 27 °C (Figure SF2); snapshot of systems used in molecular dynamics simulations − $^1H-^{13}C$ HSQC spectrum of valsartan at 27 °C (Figure SF3); $^1H-^{13}C$ HMBC spectral region (0−80 ppm) of valsartan at 27 °C (Figure SF4); $^1H-^{13}C$ HMBC spectral region (120−180 ppm) of valsartan at 27 °C (Figure SF5); spectral region (13−23 ppm) of ^{13}C (75 MHz) spectrum obtained at the temperature range of 20 to 70 °C (Figure SF6); snapshot of systems used in molecular dynamics simulations − ligand at the active site of the receptor surrounded by water molecules (top) and ligand at the active site of the receptor surrounded by DPPC bilayer and water molecules (bottom) (Figure SF7). This material is available free of charge via the Internet at http://pubs.acs.org.

REFERENCES AND NOTES

(1) De Gasparo, M.; Catt, K. J.; Inagami, T.; Wright, J. W.; Ugner, T. International Union of Pharmacology XXIII. The Angiotensin II Receptors. *Pharmacol. Rev.* **2000**, *52*, 415–472.
(2) Martin, J.; Krum, H. Role of Valsartan and other angiotensin receptor blocking agents in the management of cardiovascular disease. *Pharmacol. Res.* **2002**, *46*, 203–212.
(3) Chiolero, A.; Burnier, M. Pharmacology of Valsartan, an angiotensin II receptor antagonist. *Expert Opin. Invest. Drugs* **1998**, *7*, 1915–1925.
(4) De Gasparo, M.; Whitebread, S. Binding of Valsartan to mammalian angiotensin AT1 receptors. *Regul. Pept.* **1995**, *59*, 303–311.
(5) Fogari, R.; Zoppi, A.; Mugellini, A.; Preti, P.; Banderali, A.; Pesce, R. M.; Vanasia, A. Comparative efficacy of Losartan and Valsartan in mild-to-moderate hypertension. *Curr. Ther. Res.* **1999**, *60*, 195–206.
(6) Burnier, M. Angiotensin II Type 1 Receptor Blockers. *Circulation* **2001**, *103*, 904–912.
(7) Hedener, T.; Oparil, S.; Rasmussen, K.; Rapelli, A.; Gatlin, M.; Kobi, P.; Sullivan, J.; Oddou-Stock, P. A comparison of the angiotensin II antagonists Valsartan and Losartan in the treatment of essential hypertension. *Am. J. Hypertens.* **1999**, *12*, 414–417.
(8) Mistry, N. B.; Westheim, A. S.; Kjeldsen, S. E. The angiotensin receptor antagonist Valsartan: a review of the literature with a focus on clinical trials. *Expert Opin. Pharmacother.* **2006**, *7*, 575–581.
(9) Pool, J. L.; Schmieder, R. E.; Azizi, M.; Aldigier, J. C.; Januszewicz, A.; Zidek, W.; Chiang, Y.; Satlin, A. Aliskiren, an orally effective rennin inhibitor, provides antihypertensive efficacy alone and in combination with Valsartan. *Am. J. Hypertens.* **2007**, *20*, 11–20.
(10) Chrysant, S. G.; Chrysant, G. S. Clinical experience with angiotensin receptor blockers with particular reference to Valsartan. *J. Clin. Hypertens.* **2004**, *6*, 445–451.
(11) Kjeldsen, S. E.; Julius, S.; Arbor, A. Hypertension mega-trials with cardiovascular end points: Effect of angiotensin-converting enzyme inhibitors and angiotensin receptor blockers. *Am. Heart J.* **2004**, *148*, 747–754.
(12) Manabe, S.; Okura, T.; Watanabe, S.; Fukuoka, T.; Higaki, J. Effects of angiotensin II receptor blockade with Valsartan on pro-inflammatory cytokines in patients with essential hypertension. *J. Cardiovasc. Pharmacol.* **2005**, *46*, 735–739.
(13) Sakarellos, C.; Lintner, K.; Piriou, F.; Fermandjian, S. Conformation of the central sequence of Angiotensin II and analogs. *Biopolymers* **1983**, *22*, 663–687.
(14) Buhlmayer, P.; Furet, P.; Criscione, L.; De Casparo, M.; Whitebread, S.; Schidlin, T.; Lattmann, R.; Wood, J. Valsartan, a potent, orally active angiotensin II antagonist developed from the structurally new aminoacid series. *Bioorg. Med. Chem. Lett.* **1994**, *4*, 29–34.
(15) Angiolini, M.; Belvisi, L.; Poma, D.; Salimbeni, A.; Sciammetta, N.; Scolastico, C. Design and Synthesis of Nonpeptide Angiotensin II Receptor Antagonists Featuring Acyclic Imidazole-mimicking Structural Units. *Bioorg. Med. Chem.* **1998**, *6*, 2013–2027.
(16) Matsoukas, J.; Hondrelis, J.; Keramida, M.; Mavromoustakos, T.; Makriyannis, A.; Yamdagni, R.; Wu, Q.; Moore, G. Role of the NH2-terminal Domain of ANG II and [Sar1] ANG II on Conformation and Activity: NMR Evidence for Aromatic Ring Clustering and Peptide Backbone Folding Compared to [Des1,2,3] ANG II. *J. Biol. Chem.* **1994**, *269*, 5303–5312.
(17) Theodoropoulou, E.; Mavromoustakos, T.; Panagiotopoulos, D.; Matsoukas, J.; Smith, J. Superimposition of potent non-peptide AT1 receptor antagonists with angiotensin II. *Let. Pep. Sci.* **1996**, *3*, 209–216.
(18) Matsoukas, J. M.; Polevaya, L.; Ancas, J.; Mavromoustakos, T.; Kolocouris, A.; Roumelioti, P.; Vlahakos, D. V.; Yamdagni, R.; Wu, Q.; Moore, G. J. The Design and Synthesis of a Potent Angiotensin II Cyclic Analogue Confirms the Ring Cluster Receptor Conformation of the Hormone Angiotensin II. *Bioorg. Med. Chem. Lett.* **2000**, *8*, 1–10.
(19) Roumelioti, P.; Tselios, T.; Alexopoulos, K.; Mavromoustakos, T.; Kolocouris, A.; Moore, G. J.; Matsoukas, J. M. Structural comparison between type I and type II antagonists: possible implications in the

drug design of AT-1 antagonists. *Bioorg. Med. Chem. Lett.* **2000**, *10*, 755–758.

(20) Polevaya, L.; Mavromoustakos, T.; Zoumboulakis, P.; Grdadolnik, S. G.; Roumelioti, P.; Giatas, N.; Mutule, I.; Keivish, T.; Vlahakos, D. V.; Iliodromitis, E. K.; Kremastinos, D. T.; Matsoukas, J. Synthesis and study of a cyclic angiotensin II antagonist analogue reveals the role of pi*-pi* interactions in the C-terminal aromatic residue for agonist activity and its structure resemblance with AT(1) non-peptide antagonists. *Bioorg. Med. Chem.* **2001**, *9*, 1639–1647.

(21) Preto, M. A. C.; Melo, A.; Maia, H. L. S.; Mavromoustakos, T.; Ramos, M. J. Molecular Dynamics Simulations of Angiotensin II in Aqueous and Dimethyl Sulfoxide Environments. *J. Phys. Chem. B* **2005**, *109* (37), 17743–17751.

(22) Roumelioti, P.; Polevaya, L.; Zoumpoulakis, P.; Giatas, N.; Keivish, T.; Haritonova, A.; Zoga, A.; Vlahakos, D.; Iliodromitis, E.; Kremastinos, D.; Grdadolnik, S. G.; Mavromoustakos, T.; Matsoukas, J. Design, Synthesis and Biological Evaluation of Cyclic Angiotensin II Analogues with 3,5 Side Chain Bridges: Role of C-Terminal Aromatic Residue and Ring Cluster for Activity and Implications in the Drug Design of AT1 non Peptide Antagonists. *Bioorg. Med. Chem. Lett.* **2002**, *12*, 2627–2633.

(23) Matsoukas, J. M.; Agelis, G.; Wahhab, J.; Hondrelis, J.; Panagiotopoulos, D.; Yamdagni, R.; Wu, Q.; Mavromoustakos, T.; Maia, H. L. S.; Ganter, R.; Moore, G. J. Differences in backbone structure between angiotensin II agonists and type I antagonists. *J. Med. Chem.* **1995**, *38*, 4660–4669.

(24) Zoumpoulakis, P.; Zoga, A.; Roumelioti, P.; Giatas, N.; Grdadolnik, S. G.; Iliodromitis, E.; Vlahakos, D.; Kremastinos, D.; Matsoukas, J.; Mavromoustakos, T. Conformational and biological studies for a pair of novel synthetic AT_1 antagonists. Stereoelectronic requirements for antihypertensive efficacy. *J. Pharm. Biomed. Anal.* **2003**, *31*, 833–844.

(25) Zoumpoulakis, P.; Politi, A.; Grdadolnik, S. G.; Matsoukas, J.; Mavromoustakos, T. Structure elucidation and conformational study of V8. A novel synthetic non peptide AT_1 antagonist. *J. Pharm. Biomed. Anal.* **2006**, *40*, 1097–1104.

(26) Zoumpoulakis, P.; Grdadolnik, S. G.; Matsoukas, J.; Mavromoustakos, T. Structure elucidation and conformational properties of eprosartan a non peptide Angiotensin II AT1 antagonist. *J. Pharm. Biomed. Anal.* **2002**, *28*, 125–135.

(27) Mavromoustakos, T.; Zoumpoulakis, P.; Kyrikou, I.; Zoga, A.; Siapi, E.; Zervou, M.; Daliani, I.; Dimitriou, D.; Pitsas, A.; Kamoutsis, C.; Laggner, P. Efforts to Understand the Molecular Basis of Hypertension Trough Drug:Membrane Interactions. *Curr. Top. Med. Chem.* **2004**, *4*, 445–459.

(28) Mavromoustakos, T.; Zervou, M.; Zoumpoulakis, P.; Kyrikou, I.; Benetis, N. P.; Polevaya, L.; Roumelioti, P.; Giatas, N.; Zoga, A.; Moutevelis Minakakis, P.; Kolocouris, A.; Vlahakos, D.; Grdadolnik, S. G.; Matsoukas, J. Conformation and Bioactivity. Design and Discovery of Novel Antihypertensive Drugs. *Curr. Top. Med. Chem* **2004**, *4*, 385–401.

(29) Matsoukas, J. M.; Agelis, G.; Wahhab, A.; Hondrelis, J.; Panagiotopoulos, D.; Yamdagni, R.; Wu, Q.; Mavromoustakos, T.; Maia, H. L. S.; Ganter, R.; Moore, G. J. Differences in backbone structure between angiotensin II agonists and type I antagonists. *J. Med. Chem.* **1995**, *38* (23), 4660–4669.

(30) Mavromoustakos, T.; Theodoropoulou, E.; Dimitriou, C.; Matsoukas, J.; Panagiotopoulos, D.; Makriyannis, A. Interactions of Angiotensin II with Membranes using a combination of Differential Scanning Calorimetry and 31P-NMR spectroscopy. *LIPS* **1996**, *3* (4), 175–180.

(31) Mavromoustakos, T.; Apostolopoulos, V.; Matsoukas, J. M. Antihypertensive drugs that act on Renin-Angiotensin System with emphasis in AT1 antagonists. *Mini-Rev. Med. Chem* **2001**, *1*, 207–217.

(32) Photakis, C.; Christodouleas, D.; Chatzigeorgiou, P.; Zervou, M.; Benetis, N. P.; Vyras, K.; Mavromoustakos, T. Application of a novel CP-31P NMR methodology to study the possible interdigitation effect of losartan in phospholipids bilayers. Comparison with Raman spectroscopy data. *Biophys. J.* in press.

(33) Mavromoustakos, T.; Kolocouris, A.; Zervou, M.; Roumelioti, P.; Matsoukas, J.; Weisemann, R. An effort to understand the molecular basis of hypertension through the study of conformational analysis of Losartan and Sarmesin using a combination of nuclear magnetic resonance spectroscopy and theoretical calculations. *J. Med. Chem.* **1999**, *42*, 1714–1722.

(34) Fang, L.; Huitin, Z.; Ling, J.; Weinong, Z.; Jing, N.; Yuqi, F.; Minghui, Y.; Maili, L. Dynamic NMR study and theoretical calculations on the conformational exchange of valsartan and related compounds. *Magn. Reson. Chem.* **2007**, *45*, 929–936.

(35) Aguirre, G.; Somanathan, R.; Hellberg, L. H.; Dwyer, T. J.; North, R. N-Alkenyl amide rotational barriers by 2D EXSY NMR. *Magn. Reson. Chem.* **2003**, *41*, 131–134.

(36) Threlfall, C. C-N rotational barriers in aromatically substituted styrylformamides: an AM1 study utilizing the conductor like screening model for real solvents. *J. Mol. Struct.* **2001**, *540*, 47–52.

(37) Griesinger, C.; Ernst, R. R. Frequency Offset Effects and their Elimination in NMR Rotating-Frame Cross-Relaxation Spectroscopy. *J. Magn. Reson.* **1987**, *75*, 261–271.

(38) Mestrelab Research S.L. www.mestrec.com (accessed Jan 8, 2009).

(39) *Sybyl Molecular Modeling Software Package ver. 6.8*; Tripos Inc.: St. Louis, MO 63144, 2001.

(40) Tuccinardi, T.; Calderone, V.; Rapposelli, S.; Martinelli, A. Proposal of a New Binding Orientation for Non-Peptide AT1 Antagonists: Homology Modeling. Docking and Three-Dimensional Quantitative Structure-Activity Relationship Analysis. *J. Med. Chem.* **2006**, *49*, 4305–4316.

(41) Okada, T.; Sugihara, M.; Bondar, A. N.; Elstner, M.; Entel, P.; Buss, V. The Retinal Conformation and its Environment in Rhodopsin in Light of a New 2.2 Å Crystal Structure. *J. Mol. Biol.* **2004**, *342*, 571–583.

(42) SoftSimu; Dr. Mikko Karttunen Web page. http://www.apmaths.uwo.ca/~mkarttu/downloads.shtml (accessed Jan 8, 2009).

(43) Patra, M.; Karttunen, M.; Hyvonen, M.; Falck, E.; Lindqvist, P.; Vattulainen, I. Molecular Dynamics Simulations of Lipid Bilayers: Major Artifacts Due to Truncating Electrostatic Interactions. *Biophys. J.* **2003**, *84*, 3636–3645.

(44) Patra, M.; Karttunen, M.; Hyvonen, M.; Falck, E.; Lindqvist, P. Lipid Bilayers Driven to a Wrong Lane in Molecular Dynamics Simulations by Subtle Changes in Long-Range Electrostatic Interactions. *J. Am. Chem. Soc.* **2004**, *108*, 4485–4494.

(45) Baleanu-Gogonea, C.; Karnik, S. Model of the whole rat AT1 receptor and the ligand-binding site. *J. Mol. Model.* **2006**, *12*, 325–337.

(46) van Der Spoel, D.; Lindahl, E.; Hess, B.; Groenhof, G.; Mark, A. E.; Berendsen, H. J. GROMACS: Fast, Flexible, and Free. *J. Comput. Chem.* **2005**, *26*, 1701–1717.

(47) Van Gunsteren, W. F.; Billeter, S. R.; Eising, A. A.; Hunenberger, P. H.; Kruger, P.; Mark, A. E.; Scott, W. R. P.; Tironi, I. G. *Biomolecular Simulation: the GROMOS96 Manual and User Guide*; Vdf Hochschulverlag AG an der ETH Zurich: Zurich, 1996.

(48) Berendsen, H. J. C.; Postma, J. P. M.; van Gunsteren, W. F.; DiNola, A.; Haak, J. R. Molecular dynamics with coupling to an external bath. *J. Chem. Phys.* **1984**, *81*, 3684–3690.

(49) Essmann, U.; Perera, L.; Berkowitz, M. L.; Darden, T.; Lee, H.; Pedersen, L. G. A smooth particle mesh Ewald method. *J. Chem. Phys.* **1995**, *103*, 8577–8593.

(50) Parrinello, M.; Rahman, A. Polymorphic transitions in single crystals: a new molecular dynamics approach. *J. Appl. Phys.* **1981**, *52*, 7182–7190.

(51) Hess, B.; Bekker, H.; Berendsen, H. J. C.; Fraaije, J. G. E. M. LINCS: A linear constraint solver for molecular simulations. *J. Comput. Chem.* **1997**, *18*, 1463–1472.

(52) Humphrey, W.; Dalke, A.; Schulten, K. VMD: visual molecular dynamics. *J. Mol. Graphics* **1996**, *14*, 33–38.

(53) Microcal products. http://www.microcal.com (accessed Jan 8, 2009).

(54) Vreven, T.; Byun, K. S.; Komaromi, I.; Dapprich, S.; Montgomery, J. A.; Morokuma, K.; Frisch, M. Combining J. Quantum Mechanics Methods with Molecular Mechanics Methods in ONIOM. *J. Chem. Theory Comput.* **2006**, *2*, 815–826.

(55) (a) Lee, C.; Yang, W.; Parr, R. G. Development of the Colle-Salvetti correlation-energy formula into a functional of the electron density. *Phys. Rev. B* **1988**, *37*, 785–789. (b) Becke, A. D. Density-functional thermochemistry. III. The role of exact exchange. *J. Chem. Phys.* **1993**, *98*, 5648–5652. (c) Stephens, P. J.; Devlin, F. J.; Chabalowski, C. F.; Frisch, M. J. Ab Initio Calculation of Vibrational Absorption and Circular Dichroism Spectra Using Density Functional Force Fields. *J. Phys. Chem.* **1994**, *98*, 11623–11627.

(56) (a) Hehre, W.; Ditchfie, R.; Pople, J. Self—Consistent Molecular Orbital Methods. XII. Further Extensions of Gaussian—Type Basis Sets for Use in Molecular Orbital Studies of Organic Molecules. *J. Chem. Phys.* **1972**, *56*, 2257–2261. (b) Hariharan, P.; Pople, J. The influence of polarization functions on molecular orbital hydrogenation energies. *Theor. Chim. Acta* **1973**, *28*, 213–222. (c) Dunning, T. H., Jr. Gaussian basis sets for use in correlated molecular calculations. I. The atoms boron through neon and hydrogen. *J. Chem. Phys.* **1989**, *90*, 1007–1023. (d) Kendall, R. A.; Dunning, T. H., Jr.; Harrison, R. J. Electron affinities of the first-row atoms revisited. Systematic basis sets and wave functions. *J. Chem. Phys.* **1992**, *96*, 6796–6806.

(57) (a) Tomasi, J.; Persico, M. Molecular Interactions in Solution: An Overview of Methods Based on Continuous Distributions of the Solvent. *Chem. Rev.* **1994**, *94*, 2027–2094. (b) Amovilli, C.; Barone, V.; Cammi, R.; Cancès, E.; Cossi, M.; Menucci, B.; Pomelli, C. S.; Tomasi, J. *Adv. Quantum Chem.* **1998**, *32*, 227–261.

(58) Dewar, M. J. S.; Zoebisch, E. G.; Healy, E. F.; Stewart, J. J. P. Development and use of quantum mechanical molecular models. 76. AM1: a new general purpose quantum mechanical molecular model. *J. Am. Chem. Soc.* **1985**, *107*, 3902–3909.

(59) Frisch, M. J. ; Trucks, G. W.; Schlegel, H. B.; Scuseria, G. E.; Robb, M. A.; Cheeseman, J. R.; Montgomery, J. A., Jr.; Vreven, T.; Kudin, K. N., Burant, J. C.; Millam, J. M.; Lyengar, S. S.; Tomasi, J.; Barone, V.; Mennucci, B.; Cossi, M.; Scalmani, G.; Rega, N.; Petersson, G. A.; Nakatsuji, H.; Hada, M.; Ehara, M.; Toyota, K.; Fukuda, R.; Hasegawa, J.; Ishida, M.; Nakajima, T.; Honda, Y.; Kitao, O.; Nakai, H.; Klene, M.; Li, X.; Knox, J. E.; Hratchian, H. P.; Cross, J. B.; Adamo, C.; Jaramillo, J.; Gomperts, R.; Stratmann, R. E.; Yazyev, O.; Austin, A. J.; Camml, R.; Pomelli, C.; Ochterski, J. W.; Ayala, P. Y.; Morokuma, K.; Voth, G. A.; Salvador, P.; Dannenberg, J. J.; Zakrzewski, V. G.; Dapprich, S.; Daniels, A. D.; Strain, M. C.; Farkas, O.; Malick, D. K.; Rabuck, A. D.; Raghavachari, K.; Foresman, J. B.; Ortiz, J. V.; Cui, Q.; Baboul, A. G.; Clifford, S.; Cioslowski, J.; Stefanov, B. B.; Liu, G.; Liashenko, A.; Piskorz, P.; Komaromi, I.; Martin, R. L.; Fox, D. J.; Keith, T.; Al-Laham, M. A.; Peng, C. Y.; Nanayakkara, A.; Challacombe, M.; Gill, P. M. W.; Johnson, B.; Chen, W.; Wong, M. W.; Gonzalez, C.; Pople, J. A. *Gaussian 03 revision C,02*; Gaussian, Inc.: Pittsburgh, PA, 2004.

(60) Miura, S.; Kiya, Y.; Kanazawa, T.; Imaizumi, S.; Fujino, M.; Matsuo, Y.; Karnik, S. S.; Saku, K. Differential Bonding Interactions of Inverse Agonists of Angiotensin II Type I Receptor in Stabilizing the Inactive State. *Mol. Endocrinol.* **2008**, *21*, 139–146.

(61) Takezako, T.; Cogonea, C.; Saad, Y.; Noda, K.; Karnik, S. S. "Network leaning" as a mechanism of insourmountable antagonism of angiotensin II type I receptor by non-peptide antagonism. *J. Biol. Chem.* **2004**, *279*, 15248–15257.

CI800427S